SPE-210228-MS

Effect of Supercritical CO_2 on the Poroelastic Characteristics of Poorly Cemented Sandstone Reservoirs During Depletion and Injection

Sam S Hashemi, Anthony R Kovscek, and Mark D Zoback, Stanford University

This paper was prepared for presentation at the 2022 SPE Annual Technical Conference and Exhibition held in Houston, Texas, USA, 3 - 5 October 2022.

Abstract

While there is continuing interest in geologic CO_2 storage, experimental studies on poroelastic characteristics of reservoir rocks during depletion and subsequent CO_2 injection are scarce. Rock stiffness, confining stress, and pore pressure control the poroelastic response of saturated rocks. Also, the stress and pore pressure evolution during injection is a key parameter to understanding operations thresholds for CO_2 storage projects. As depleted fields in the Gulf of Mexico have been identified as strong candidates for CO_2 storage projects, it is important to understand if the poroelastic characteristics from such fields have been altered due to depletion. Among rock properties, Young's modulus (E), bulk modulus (K_b) and Biot coefficient (α) are of particular importance.

In this study, the poroelastic deformation of a core from the West Delta field in the Gulf of Mexico is characterized experimentally and the impacts of supercritical CO_2 ($scCO_2$) on the specimen are investigated. The experimental program simulated reservoir stress changes due to production-induced depletion and $scCO_2$ injection through cycling both the confining pressure (C_p) and pore pressure (P_p). We measured the deviatoric stress, volumetric strain, derived the corresponding Young's (E), bulk moduli (K_b) and Biot coefficient (α). The results show that the effect of $scCO_2$ on E is more significant at greater confining pressures during the injection phase than depletion at a constant simple effective stress. Interaction of $scCO_2$ with clay minerals caused rock frame dehydration and led to an increase in E. The bulk modulus increased with increasing the confining pressure at a given P_p and decreased with P_p at a certain C_p. α rose with P_p during both depletion and injection phases. Interaction with $scCO_2$ limited the variation of α and the effect of P_p and C_p on α decreased in significance during the depletion phase. Longer interaction time with $scCO_2$ increased α from 10-25% at different P_p values compared to argon during the injection stage. However, the influence of effective stress in reducing the α weakened.

Introduction

CO_2 storage in geological formations shows great potential as a pathway to reduce greenhouse gas emissions. Nevertheless, investigating the feasibility, injectivity, and risks associated with storage is necessary to ensure long-term and safe CO_2 storage (Raziperchikolaee et al., 2021). It is well known that the

deformation of saturated reservoir rock is dependent on in-situ stresses, pore pressure, and the rock elastic moduli. Depending on the rock type, the effect of pore pressure and stresses on rock deformation vary. The type of fluids may also influence the poroelastic characteristics of rocks.

The production of hydrocarbons from reservoirs reduces reservoir pore pressure, potentially causing compaction of both the reservoir and overlying caprock, such as the Groningen gas field, Netherlands (van Thienen-Visser & Breunese, 2015). When CO_2 is injected, it causes the pore pressure to increase and potentially displaces the in-situ pore fluids. This pressure perturbation can go beyond that of its original conditions of pre-hydrocarbon extraction resulting in significant stress and deformation in and around the storage reservoir (Hosseininoosheri et al., 2018; Ringrose et al., 2013). These stress changes within the reservoir could lead to a change in rock properties such as porosity, permeability and injectivity potential (Chan & Zoback, 2002; Segall, 1985). Such changes could generate new fractures or reactivate pre-existing faults in both the reservoir and caprocks, leading to surface uplift, induced seismicity, and CO_2 leakage into subsurface water resources (Raziperchikolaee & Pasumarti, 2020).

The effective stress (σ') is widely used to evaluate the net effect of confining pressure and pore pressure on rock deformation (Biot, 1962; von Terzaghi, 1923). The Biot coefficient (α) was defined to describe the interaction between pore pressure and solids deformation within a porous medium. In fact, α quantifies the rock's susceptibility to pore pressure and it helps us to understand the reservoir's effective stress, its changes, and associated deformation. Different approaches have been suggested to improve the accuracy and efficiency of the measurement of α because it is the key factor to calculate effective stress precisely. A conventional technique to calculate the Biot coefficient was presented by (Skempton, 1961) as follows

$$\alpha = 1 - K_b / K_g \tag{1}$$

where K_b is the bulk modulus of the rock and K_g is the solid rock grain bulk modulus. In this method, two different experiments are required for estimating the K_b and K_g. In the first test, K_b is obtained by adjusting the pore pressure to zero; and in the subsequent test, by setting the confining pressure and pore pressure to equal values, K_g can be calculated.

The poroelastic responses of tight sandstones and a North Sea chalk were measured by Warpinski & Teufel, (1992). They showed that α for deformation in those rocks is less than unity and that it decreases with confining pressure and increases with pore pressure. Franquet & Abass, (1999) experimentally tested different reservoir sandstones and found α dropped as the confining pressure increased. Ojala & Sønstebø, (2010) also tested Pierre shale and showed that α consistently declines from 1 as confining pressure increases. Ma & Zoback, (2017b) characterized Middle Bakken tight sandstones to investigate the dependencies of α on confining pressure and pore pressure. Their results showed that the Biot coefficient was less than unity, and typically varied between 0.3 and 0.8.

Although there is an ongoing interest in CO_2 storage in underground geologic formations, the experimental investigations of poroelastic responses of a reservoir during depletion and subsequent CO_2 injection are rarely found in the literature. Here, we characterize the poroelastic deformation of a core from the West Delta field in the Gulf of Mexico. We simulate reservoir stress changes due to depletion and $scCO_2$ injection through cycling both the confining pressure (C_p) and pore pressure (P_p). The impacts of $scCO_2$ on Young's (E) and bulk moduli (Kb) and Biot coefficient (α) are investigated and rationalized.

West Delta core

The West Delta specimen (SN10) used in this study was extracted from a vertical well at ~2.3-km depth, perpendicular to bedding planes. The extended XRD analysis of the specimen is shown in Table 1. It shows that specimen SN10 is clay-rich and contains 22.3% of expandable clay including smectite and illite. The initial porosity of SN10 is 23.1%, and the matrix permeability was measured at a confining pressure of 5.51 MPa using nitrogen. The absolute and Klinkenberg permeabilities are 5.12 mD and 3.81 mD, respectively.

The core was prepared into a cylindrical specimen of 2-inch length and 1-inch diameter, with both ends grounded flat and parallel.

Table 1—XRD analysis of the specimen SN10

Depth (km)	QFP* (%)	Carbonates (%)	Clay + TOC (%)	Expandable clay % (of total clay) **
2.31	40.90	4.50	54.70	22.30

*Quartz + Feldspar + Pyrite

**Smectite and illite

According to Zoback, (2010), fields in the Gulf of Mexico have a stress gradient of $S_{Hmax}/S_{hmin}/S_v$ #13.8/13.8/23 MPa/km. Therefore, the mean stress at the depth of 2.3 km where the core was extracted is approximately 39 MPa. The pore pressure gradient in this field is hydrostatic (10 MPa/km), and that yields a P_p of 22.7 MPa at the depths of coring. These construed magnitudes of in-situ mean stress and P_p set realistic values to which our loading path design refers.

Experimental procedure

The experiments were performed using a triaxial testing system. The specimens were jacketed using a 0.75mm-thick heat-shrink Viton sleeve, which was then sealed on two steel core-holders using flexible steel wires. The confining pressure was measured using a Heise DXD pressure transducer accurate to ±0.1% up to 90 MPa. The pore pressure tubes were connected to the sample through core-holders and pore pressure was controlled by a Quizix 6000 pump, using two independent cylinders with argon and $scCO_2$ as pore fluids (Fig. 1). The pumps, that measure pressures with an accuracy of ±0.3% of the full scale and deliver pressures up to 50 MPa, were used to measure pore pressures and control flow rates.

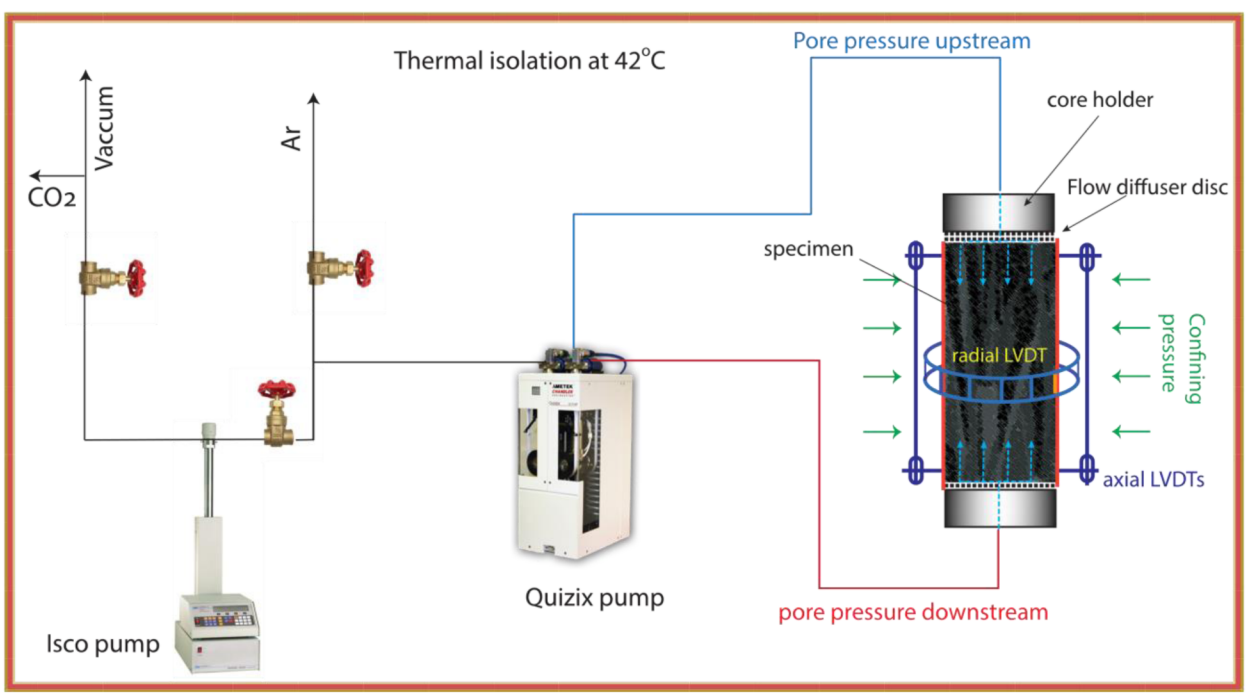

Figure 1—Schematic diagram of the experimental setup. The system allows true triaxial stress conditions to be applied.

Because the CO_2 state is very susceptible to temperature change, four heaters, three thermostats, and a fan were installed inside the chamber to insulate thermally the chamber and keep and distribute a constant temperature of 42°C (±0.2°C). A temperature probe was used to monitor the temperature at several locations inside the chamber during the tests. Two vertical and one radial chain LVDT (linear variable differential transformer) sensors were used to record the axial and radial deformation. The recorded deformations (axial and lateral) were used to compute Young's modulus (E), volumetric strain (ε_v) and static bulk modulus (Kb), leading to the evaluation of the Biot coefficient (α).

The specimen was initially subjected to hydrostatic confining pressure (C_P) under drained conditions, simulating the stressed rock in-situ as depletion occurs. The overall experimental sequence that varied confining pressure and pore fluid pressure as a function of time is shown in Fig. 2. The loading path was designed in a way for the specimen to experience possible combinations of C_p and P_p when exposed to argon and $scCO_2$. C_p and P_p were allowed to slightly go beyond the estimated in-situ stresses and pore pressure in order to replicate both injection and depletion phases.

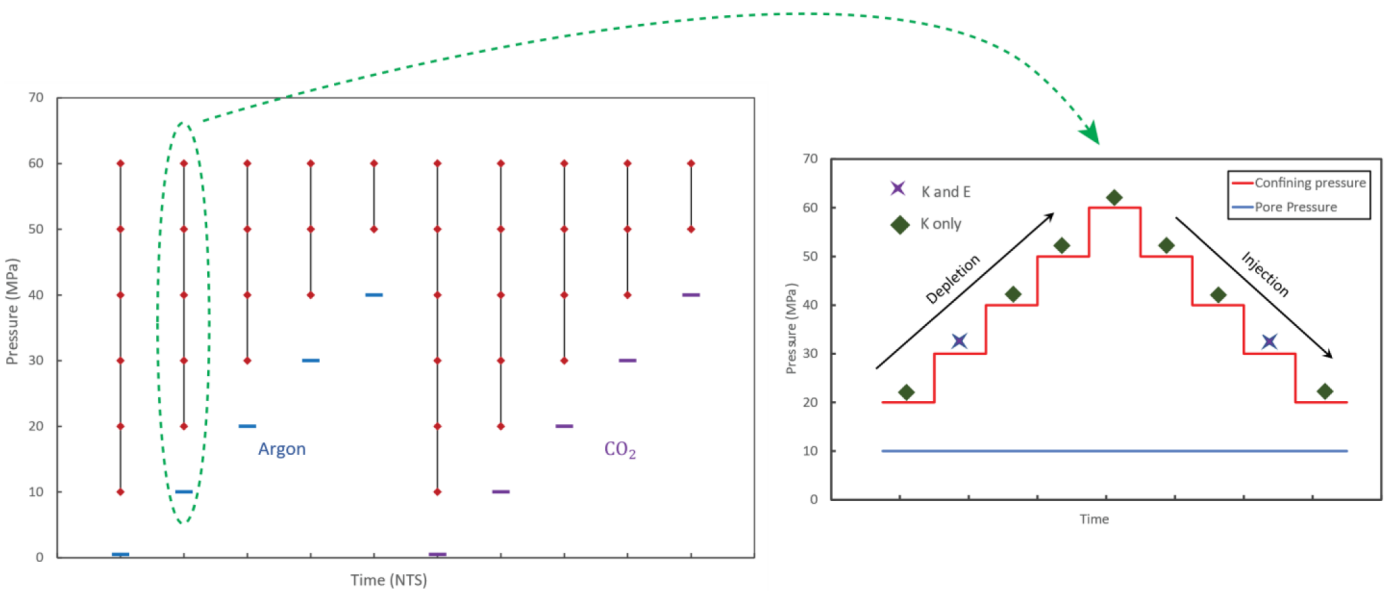

Figure 2—Stress-loading paths followed during measurements.

The condition of the loading C_p with constant P_p is representative of the depletion phase, while the condition of unloading P_c simulates injection. For a given P_p, C_p is increased to a maximum of 60 MPa and back to a minimum of 10 MPa, Fig. 2. The pore pressure was increased stepwise from 10 MPa to 40 MPa and the deformation was measured at each step. Then, the pore pressure was lowered to 10 MPa and the above cycle was repeated. The same measurements were performed at each pore pressure in the injection process. Then, P_p was increased to the next level and C_p was cycled accordingly. For each step of C_p and P_p, adequate waiting time was allowed for the P_p to reach equilibrium. Upon stabilizing the moving LVDT readings, equilibrium was considered complete. Afterwards, argon pore pressure was removed, and the specimen/tubes were vacuumed for 24 hours to remove any residual argon. $scCO_2$ was then introduced into the sample and allowed to equilibrate for 24 hours. The same cycle of P_p and C_p as that of argon was applied and deformation measurements were made. The temperature in the chamber was set at ~ 42°C to ensure that CO_2 was maintained in the supercritical state.

Poroelastic deformation

Firstly, the specimens were subjected to a seasoning procedure (Rassouli & Zoback, 2018) that cycled between 5 and 60 MPa confining pressure three times with zero pore pressure. The purpose of cycling was to ensure that some relaxation microcracks and pores closed. Fig. 3 shows the $C_p - \varepsilon_v$ responses of the specimen. The slope of each curve represents the static bulk modulus (Kb). With increasing the C_p, K_b rose consistently in the first loading cycle. Compaction of clay minerals is thought to result in stiffening of the specimen with confining pressure. K_b variation with C_p was reduced in the first unloading cycle. Most of the inelastic deformation occurred during the first loading-unloading cycle. Following the second and third seasoning cycles, the trends of the stress-strain curves were similar, except that each cycle applied greater inelastic compaction that appears to decrease with the number of cycles. After the 3rd cycle, we considered the seasoning process completed and commenced the main testing program.

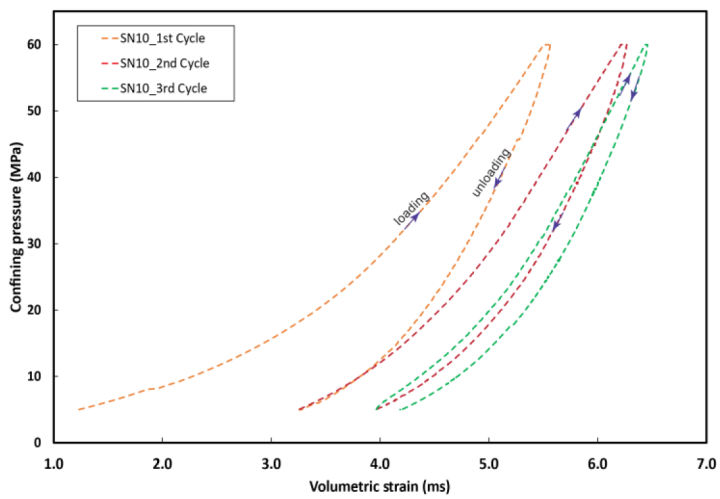

Figure 3—Three seasoning cycles and $C_p - \varepsilon_v$ responses. Note the closing of loading and unloading curves with 3 cycles.

The test results under the designated loading path were analyzed in order to estimate the elastic moduli including static bulk and Young's moduli. Then the variation of volumetric strain with respect to C_p and P_p was considered to calculate the Biot coefficient. Fig. 4 shows the volumetric strain versus confining pressure response of the West Delta specimen under different constant pore pressures for argon and $scCO_2$. The color lines are fitted to the constant P_p data series. Constant P_p data series are highlighted and fitted with contour lines of the corresponding color. The effect of confining pressure C_p is observed by these trend lines. Constant simple effective stress σ' (= C_p-P_p) data series are shown with dashed green contour lines. Based on these lines of data, it appears that C_p and P_p counteract each other's influence on effective stress. P_p reduces the volumetric strain by weakening the effect of confinement, C_p, on the rock matrix. The inclined constant effective stress curve indicates that P_p does not cancel out C_p effects completely.

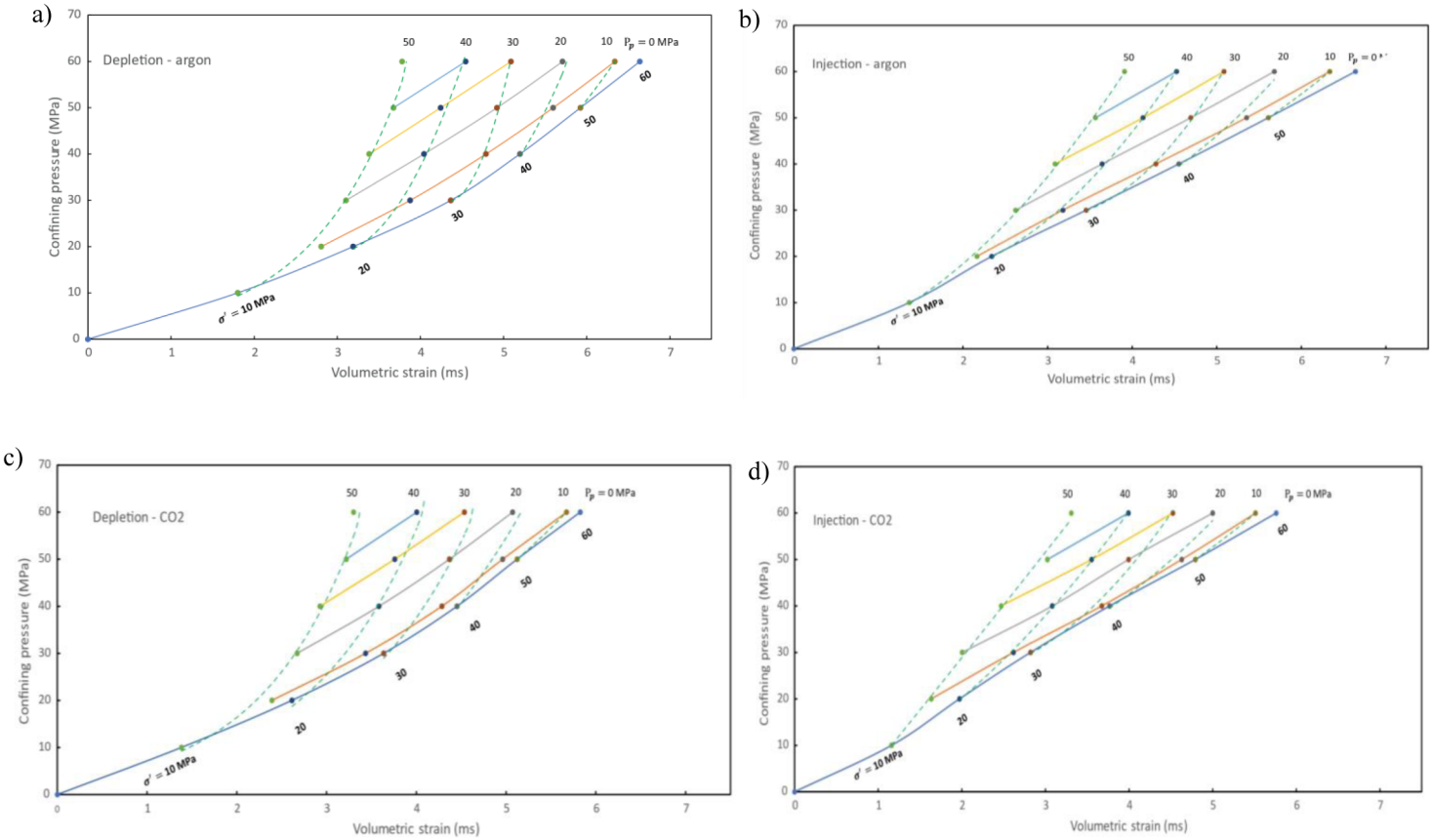

Figure 4—$C_p - \varepsilon_v$ response of the core under constant pore pressure during loading (depletion phase) and unloading (injection phase); a) argon depletion, b) argon injection, c) $scCO_2$ depletion, d) $scCO_2$ injection.

Fig. 4 (a) and (b) show the argon depletion (loading C_p) and injection (unloading C_p) stages, respectively. The disparity between the two phases is attributed to loading unloading/hysteresis of the material. In the depletion phase, for each constant P_p, the stress-strain curve seems to be non-linear up to the maximum C_p applied. This is better illustrated in Fig. 5 where the range of bulk modulus is quite wide. It ranges from 6.35 to 10.68 GPa (i.e., 68% increase). Thus, unlike hard rocks such as Middle Bakken cores (Ma & Zoback, 2017a), the stiffness of the clay-rich West Delta rock is influenced by confining pressure.

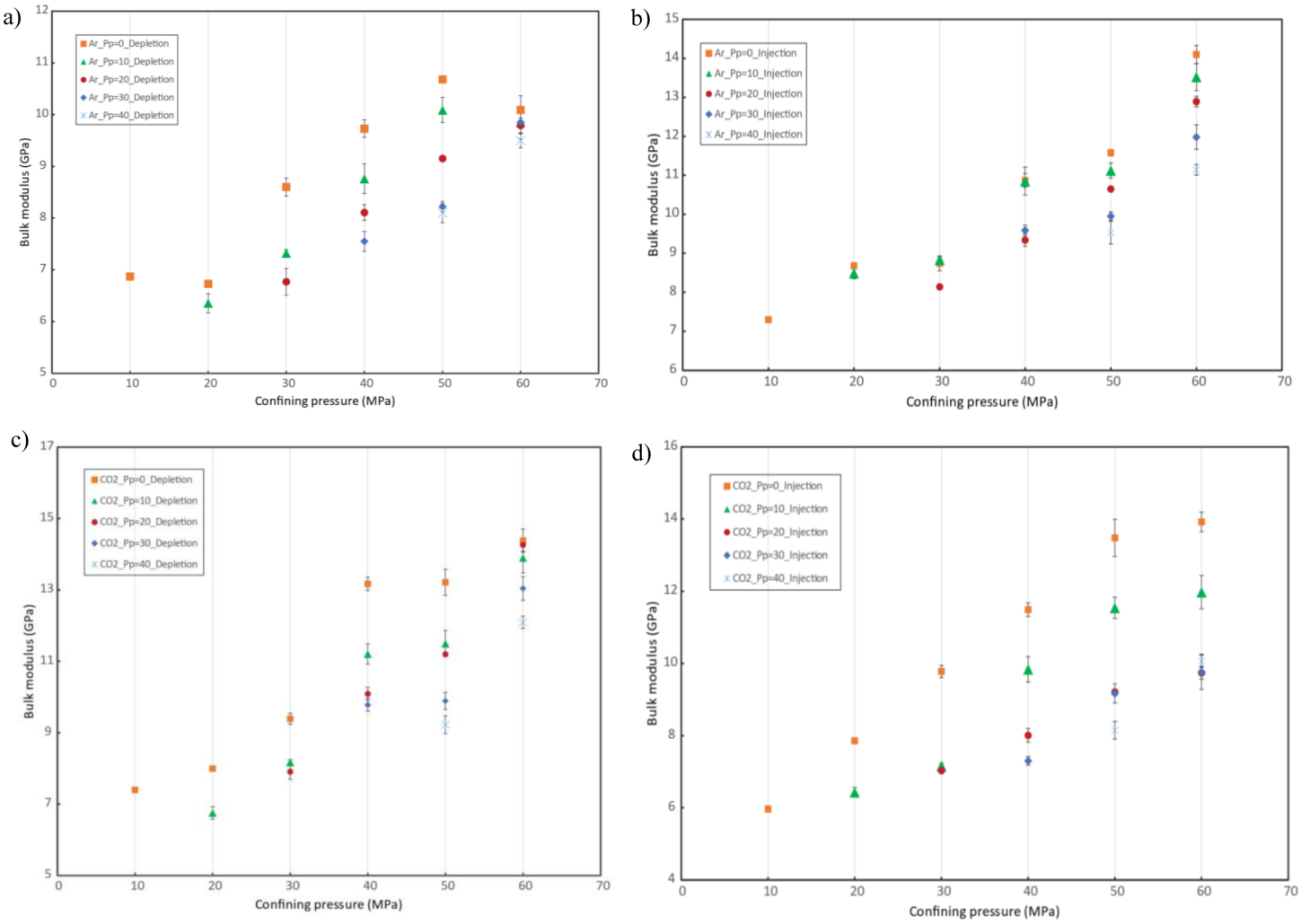

Figure 5—Variation of bulk modulus with confining pressure under constant pore pressure levels during loading (depletion stage) and unloading (injection stage): a) argon depletion b) argon injection c) $scCO_2$ depletion d) $scCO_2$ injection.

These data series show an opposite effect of C_p and P_p on volumetric strain evolution. In addition, the stress-strain curves of all constant $P_p$values align nearly sub-parallel to one another. This implies the rock stiffness is barely affected by the pore pressure. The effect of pore pressure on effective stress might be examined by constant simple effective stress σ'contours.

As mentioned before, P_p alleviates the confining effect of C_p on the rock frame, as higher P_p results in decreasing ε_v. However, an inclined constant σ' curve suggests that the internal P_p does not completely cancel the external compression of C_p. For a constant σ', a non-linear response shows that the Biot coefficient (α) changes with rising the P_p. For instance, the σ' = 10 MPa trend consistently curves upward as P_p rises, suggesting that α gets closer to 1 at a greater P_p.

Figs. 4 (c) and (d) illustrate the depletion and injection phases when $scCO_2$ was used as the pore fluid. The offset between constant P_p lines generally increase as P_p increases, suggesting a non-linear P_p-effect on counteracting the C_p confinement. It is obvious from Fig. 4c that volumetric strain does not remarkedly change when the pore pressure increases from 0 to 10 MPa in both depletion and injection stages during the $scCO_2$ phase. This was not the case in the argon stage and may be due to the effect of remaining $scCO_2$ within the pores when testing the specimen at $P_p = 0$. Please note that we did not vacuum the specimen at P_p=0. The pore pressure valves were left open, and deformation measurements were made in the drained condition.

If the P_p and σ' curves were linear, the relative contribution of C_p and P_p on effective stress coefficient is fixed and the α is unchanged. The combination of non-linear constant P_p and σ' curves indicates the α varies when changing the C_p and P_p. Figure 4 also illustrates the variation in the trend of constant σ' for constant pore pressure. For constant C_p, the local tangent of constant σ' curve increases as σ' decreases. This yields a rising Biot coefficient with decreasing effective stress. α will ideally achieve its maximum when the strain does not change when C_p and P_p increase equally $\left(\frac{\partial P_p}{\partial \varepsilon_v} \approx \infty\right)$. That is, $C_p = P_p$, and the pore pressure is applied, and the strain measurement takes the rock's frame deformation, yielding the bulk modulus of a single grain.

The injection phase is different from the depletion. The specimen stiffened as C_p increase under a constant P_p. the rise of pore pressure for constant C_p softens the specimen, as shown in Fig. 5. The bulk modulus in the $scCO_2$ depletion phase is higher than that of the argon depletion phase. This may be due to multiple loading and unloading cycles leading to porosity reduction. $ScCO_2$ also dehydrates the sample and causes it to become stiffer. A longer interaction time with $scCO_2$, however, reduced the bulk modulus. This implies that the effect of porosity reduction in increasing K_b is less than the effect of the interaction of $scCO_2$ with clay minerals that causes stiffness reduction. On the other hand, because the stress magnitude during $scCO_2$ was the same as the argon cycle, the sample did not sit on a new $p'^{\#}$ (i.e., past maximum effective stress that the rock experienced in the field) and that implies the porosity did not significantly change (assuming no hysteresis during cycles) during $scCO_2$ depletion and injection phases.

The constant σ' curves are more linear during the injection phase than depletion. This suggests a small variation of α with increasing the pore pressure. In the last section, we determined the variation of α with C_p and P_p when the specimen was exposed to argon and $scCO_2$.

Young's modulus

The Young's modulus of the specimen was measured using the tangent method at different C_p and P_p magnitudes both for argon and $scCO_2$ at a constant simple effective stress of 20 MPa. The error bar illustrates the range of E at any stress condition (C_p, P_p) we applied along the loading path. The variations of E with C_p and P_p are displayed in Fig. 6.

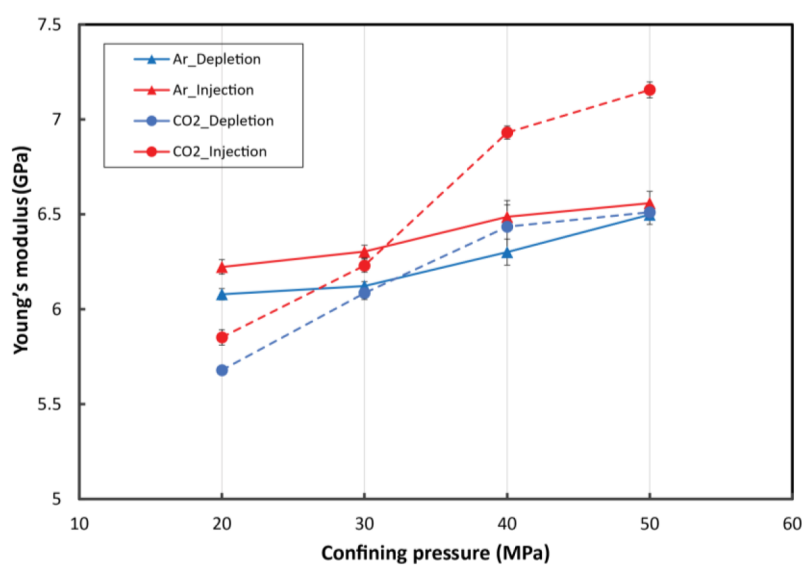

Figure 6—Variation of Young's Modulus with confining pressure under constant effective stress (20 MPa) conditions during depletion and injection phases

Argon was initially used as the pore fluid, and then $scCO_2$ was introduced to the specimen to identify its effect on E during the depletion and injection phases. In general, E was always slightly greater during injection than during depletion for the same C_p and P_p condition. The range of E changes was greater during injection than that of depletion, especially in the $scCO_2$ phase. E rose as the confining pressure increased in both depletion and injection phases. Pore fluid type did not alter this trend.

When argon was vacuumed out and the specimen was exposed to $scCO_2$ for 24 hours, E reduced about 13.5% at the C_p = 20 MPa and P_p=0 MPa. As the pore pressure increased to 10 MPa (at C_p =30 MPa) E retrieved, almost equal to the argon depletion phase. However, E increased about 9.25% at C_p=50 MPa during the $scCO_2$ injection phase. This stiffening may be due to the absorption of $scCO_2$ into clay minerals and dehydrating the specimen matrix. Bai et al., (2021) tested the clay-rich shales exposed to $scCO_2$ and showed that adsorption of $scCO_2$ increases Young's modulus. They also showed that adsorption reduced the strength of samples and that was a dominant factor in improving Young's modulus.

Biot coefficient derivations

Todd & Simmons, (1972) experimentally studied the effects of C_p and P_p on wave velocities. Sarker & Batzle, (2008) extended their method of calculating α to other physical properties and suggested the following:

$$\alpha = 1 - \frac{\left(\frac{\partial Q}{\partial P_p}\right)_{\sigma'_{constant}}}{\left(\frac{\partial Q}{\partial \sigma'}\right)_{P_{p_{constant}}}} \tag{2}$$

where Q is an arbitrary measured physical entity and σ' is the simple effective stress. Ma & Zoback, (2017a) used Eq. 2 in their study and suggested that in the case of static α, the measured physical quantity Q is specified to be the volumetric strain. To be consistent with the definition of bulk modulus, Eq. 2 was rearranged to the following equation for estimating the static Biot coefficient:

$$\alpha = 1 - \frac{\left(\frac{\partial \sigma'}{\partial \varepsilon_v}\right)_{P_{p_{constant}}}}{\left(\frac{\partial P_p}{\partial \varepsilon_v}\right)_{\sigma'_{constant}}} \tag{3}$$

Equation 3 teaches that if the specimen is tested under an unjacketed condition ($C_p = P_p$), the denominator in Eq. (2) turns into $d\ (P_p)/d\ (\varepsilon v)$. Theoretically, this equals K_g and is a function of P_p. The numerator in Eq. (3) changes to the bulk modulus of the rock (Kb) when the specimen is jacketed ($C_p > P_p$) and drained condition at varying pore pressure levels as $d\ (\sigma) = d\ (C_p)$. In fact, Eq. (1) is a special case of Eq. (3) when the no effective stress is applied and the denominator in the latter is equal to K_g.

Ma & Zoback, (2017a) showed that Eq. (3) is more accurate because effective stress is larger than 0 in most jacketed tests and α measures the relative contribution of C_p and P_p to the actual effective stress, at a certain (C_p, P_p) condition. On the other hand, the equation suggested by Todd & Simmons, (1972) defines α as a dependent of both C_p and P_p. It is worth mentioning that in studies where measured velocities are used to derive the dynamic Biot coefficient (Hornby, 1996; Sarker & Batzle, 2008), the amount of the induced strain is a few orders of magnitude less than measured during static conditions (Mavko et al., 2020). The dynamic measurements do not consider the induced inelastic deformation either. Because the reservoir deformation associated with depletion and $scCO_2$ injection generally involves both elastic and plastic strain, the Biot coefficients estimated from static tests are more suitable in the reservoir simulations.

We calculated α using the local tangent to the curves of constant σ' and P_p at each pore pressure and confining pressure. Fig. 7 shows the α variations when argon and $scCO_2$ were used as pore fluids at different effective stress magnitudes. Generally, α rises when increasing the P_p at a given C_p and the maximum α is

achieved when P_p reaches its larges value. This corresponds to the minimum effective stress. On the other hand, α decreases with increasing effective stress. The effect of C_p on reducing α is observed in Fig. 7a and 7b. The trend of variation of α is similar in both argon depletion and injection phases, and it is always less than unity. It is clear that the α is more susceptible to P_p changes than that of C_p. This result agrees with the outcome of the bulk modulus analysis in the previous section.

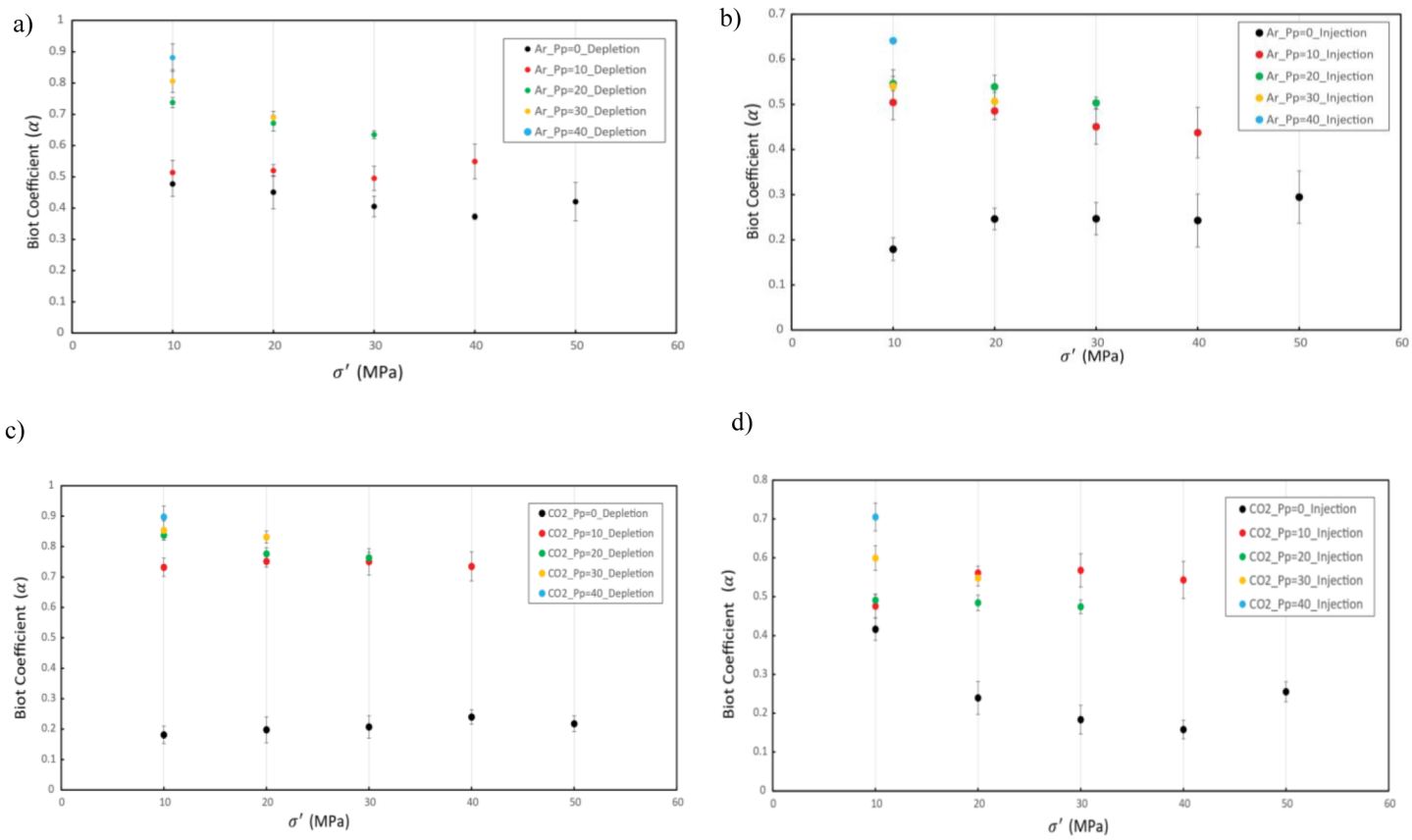

Figure 7—Variations of Biot coefficient with simple effective stress for constant pore pressures under depletion and injection stages: a) argon depletion b) argon injection c) $scCO_2$ depletion d) $scCO_2$ injection.

α varied between ±0.10 under constant P_p, but it changed up to 0.71 under constant effective stress conditions. For instance, when P_p varies from 0 to 40 MPa, α increases from ~0.37 to ~0.88 when effective stress is 10 MPa during the argon depletion phase. When $scCO_2$ was introduced to the sample, α decreased dramatically to 0.18 at $P_p = 0$. However, when the P_p increased, α increased and a similar trend to argon depletion was observed during the $scCO_2$ depletion phase.

As shown in Fig. 7b, α decreased during the argon injection phase and ranges from 0.18 to 0.64 when the specimen was unloaded. $ScCO_2$ did not change this trend during the injection phase (Fig. 7d), and the range of variation of α was 0.16 at $P_p = 0$ and 0.70 at $P_p = 40$ MPa. These values are slightly greater than that of argon at the same P_p. Interaction with $scCO_2$ limited the variation of α and the effect of P_p and C_p in changing α weakened.

The variation of α with C_p and P_p implies that the modeling of reservoir stress and pore pressure evolution using a constant α might not reflect the actual reservoir response. α plays an important role in the poroelastic responses of a potential reservoir for CO_2 sequestration. It changes after a reservoir is depleted. Thus, α should be used cautiously in analytical and numerical models to predict properly reservoir behavior during/after CO_2 injection. How minimum horizontal stress and pore pressure evolve during CO_2 injection determines whether local pore pressure build-up reactivates any nearby faults within or outside the reservoir.

Conclusion

A series of drained experiments was conducted on a West Delta reservoir core using argon and $scCO_2$ as pore fluids. The stress-volumetric strain responses showed a significant pore pressure effect, in addition to the confining pressure effect on rock poroelastic characteristics.

Young's modulus increased as the confining pressure increased in both depletion and injection stages. Interaction with $scCO_2$ did not change this trend. However, E increased after the specimen was exposed to $scCO_2$ for almost 20 days during the injection phase. This stiffening may be due to the absorption of $scCO_2$ into clay minerals and specimen dehydration.

The bulk modulus increased with C_p significantly under a constant P_p (up to 133% during $scCO_2$ injection phase), while the rise of pore pressure for constant C_p softens the specimen. Results showed that K_b in the $scCO_2$ depletion phase was greater than that of the argon phase. This is due to multiple loading and unloading cycles leading to porosity reduction and inelastic compaction. When, however, the specimen was exposed to $scCO_2$ for a longer period, K_b was reduced. The opposite trend of E and K_b in the presence of $scCO_2$ indicates that greater deformation occurred in the lateral direction than axial. The specimen was cored from a vertical core where the bedding planes were perpendicular to the core axis.

The calculated Biot coefficient increased with pore pressure despite constant effective stress. This suggests that the overall effect of P_p on compensating the induced compaction caused by C_p was enhanced. The derived α values were persistently less than unity regardless of pore fluid type and stress condition. Measured α varied between 0.18 to 0.89 during the $scCO_2$ depletion phase; however, α reduced during the $scCO_2$ injection phase and it ranged from 0.16 to 0.70. Exposure to $scCO_2$ for a longer period increased α from 10-25% at different P_p values compared to argon during the injection stage. However, the influence of effective stress in reducing the α decreased.

Because α plays an important role in the poroelastic characteristics of a candidate depleted reservoir for CO_2 storage, one should consider using precise values in analytical and numerical models. This determines how minimum horizontal stress and pore pressure evolve during CO_2 injection and whether rising local pore pressure reactivates any nearby faults. We plan to extend the experiments to another three West Delta cores from the same wellbore but at different depths and mineral compositions. Test results will be used to simulate the stress and pore pressure variations.

Acknowledgements

This work was supported by ExxonMobil through the Strategic Energy Alliance at Stanford University and the Stanford Center for Carbon Storage.

References

Bai, B., Ni, H., Shi, X., Guo, X., & Ding, L. (2021). The experimental investigation of effect of supercritical CO 2 immersion on mechanical properties and pore structure of shale. *Energy*, **228**, 120663. https://doi.org/10.1016/j.energy.2021.120663

Biot, M. A. (1962). Mechanics of deformation and acoustic propagation in porous media. *Journal of Applied Physics*, **33**(4), 1482–1498.

Chan, A. W., & Zoback, M. D. (2002). Deformation analysis in reservoir space (DARS): a simple formalism for prediction of reservoir deformation with depletion. SPE/ISRM Rock Mechanics Conference.

Franquet, J. A., & Abass, H. H. (1999). Experimental evaluation of Biot's poroelastic parameterThree different methods. Vail Rocks 1999, The 37th US Symposium on Rock Mechanics (USRMS).

Hornby, B. E. (1996). An experimental investigation of effective stress principles for sedimentary rocks. In *SEG Technical Program Expanded Abstracts 1996* (pp. 1707–1710). Society of Exploration Geophysicists.

Hosseininoosheri, P., Hosseini, S. A., Nuñez-López, V., & Lake, L. W. (2018). Impact of field development strategies on CO2 trapping mechanisms in a CO2–EOR field: A case study in the permian basin (SACROC unit). *International Journal of Greenhouse Gas Control*, **72**(April), 92–104. https://doi.org/10.1016/j.ijggc.2018.03.002

Ma, X., & Zoback, M. D. (2017a). *Journal of Geophysical Research : Solid Earth*. 2478–2503. https://doi.org/10.1002/2016JB013668

Ma, X., & Zoback, M. D. (2017b). Laboratory experiments simulating poroelastic stress changes associated with depletion and injection in low-porosity sedimentary rocks. *Journal of Geophysical Research: Solid Earth*, **122**(4), 2478–2503. https://doi.org/10.1002/2016JB013668

Mavko, G., Mukerji, T., & Dvorkin, J. (2020). *The rock physics handbook*. Cambridge university press.

Ojala, I. O., & Sønstebø, E. F. (2010). The effective stress coefficient in Pierre shale. AAPG Hedberg Conference.

Rassouli, F. S., & Zoback, M. D. (2018). Comparison of Short-Term and Long-Term Creep Experiments in Shales and Carbonates from Unconventional Gas Reservoirs. *Rock Mechanics and Rock Engineering*, **51**(7), 1995–2014. https://doi.org/10.1007/s00603-018-1444-y

Raziperchikolaee, S., Cotter, Z., & Gupta, N. (2021). Assessing mechanical response of CO2 storage into a depleted carbonate reef using a site-scale geomechanical model calibrated with field tests and InSAR monitoring data. *Journal of Natural Gas Science and Engineering*, **86**(December 2020), 103744. https://doi.org/10.1016/j.jngse.2020.103744

Raziperchikolaee, S., & Pasumarti, A. (2020). The impact of the depth-dependence of in-situ stresses on the effectiveness of stacked caprock reservoir systems for CO2 storage. *Journal of Natural Gas Science and Engineering*, **79**, 103361.

Ringrose, P. S., Mathieson, A. S., Wright, I. W., Selama, F., Hansen, O., Bissell, R., Saoula, N., & Midgley, J. (2013). The In Salah CO2 storage project: lessons learned and knowledge transfer. *Energy Procedia*, **37**, 6226–6236.

Sarker, R., & Batzle, M. (2008). Effective stress coefficient in shales and its applicability to Eaton's equation. *The Leading Edge*, **27**(6), 798–804.

Segall, P. (1985). Stress and subsidence resulting from subsurface fluid withdrawal in the epicentral region of the 1983 Coalinga earthquake. *Journal of Geophysical Research: Solid Earth*, **90**(B8), 6801–6816.

Skempton, A. W. (1961). Horizontal stresses in an overconsolidated Eocene clay. *SELECTED PAPERS ON SOIL MECHANICS*, 119.

Todd, T., & Simmons, G. (1972). Effect of pore pressure on the velocity of compressional waves in low-porosity rocks. *Journal of Geophysical Research*, **77**(20), 3731–3743.

van Thienen-Visser, K., & Breunese, J. N. (2015). Induced seismicity of the Groningen gas field: History and recent developments. *The Leading Edge*, **34**(6), 664–671.

von Terzaghi, K. (1923). Die Berechnung der Durchassigkeitsziffer des Tones aus dem Verlauf der hydrodynamischen Spannungs. erscheinungen. *Sitzungsber. Akad. Wiss. Math. Naturwiss. Kl. Abt*. **2A**, 132, 105–124.

Warpinski, N. R., & Teufel, L. W. (1992). Determination of the effective-stress law for permeability and deformation in low-permeability rocks. *SPE Formation Evaluation*, **7**(02), 123–131.

Zoback, M. D. (2010). *Reservoir geomechanics*. Cambridge University Press.